Materials Research Bulletin 108 (2018) 113–119

Contents lists available at ScienceDirect

Materials Research Bulletin

journal homepage: www.elsevier.com/locate/matresbu

Lead free, air stable perovskite derivative Cs_2SnI_6 as HTM in DSSCs employing TiO_2 nanotubes as photoanode

Lekha Peedikakkandy[a,*], Johns Naduvath[b,c], Sudhanshu Mallick[c], Parag Bhargava[c,*]

[a] Center for Research in Nanotechnology and Science, Indian Institute of Technology-Bombay, Powai, Mumbai-76, India
[b] Department of Physics, St. Thomas College (Autonomous), Thrissur, Kerala, India
[c] Department of Metallurgical Engineering and Materials Science, Indian Institute of Technology-Bombay, Powai, Mumbai-76, India

ARTICLE INFO

Keywords:
Lead free perovskite
Titania nanotubes
Solid State DSSC

ABSTRACT

Cs_2SnI_6 is an air-stable and non-toxic perovskite variant photovoltaic material which exhibits p-type conductivity under doped conditions. In this work, we report the synthesis and stability studies of Cs_2SnI_6 towards its application as a solid-state Hole Transport Material (HTM) in Titania Nanotube (TNT) based Dye Sensitized Solar Cells (DSSCs). Cs_2SnI_6 crystals were synthesized using precipitation method and its stability was assessed using X-ray diffraction (XRD), X-ray Photoelectron Spectroscopy (XPS) and Thermogravimetric Analysis (TGA). Cs_2SnI_6 doped with SnI_2 was deposited onto the TNT photo-anode as the HTM layer through dip coating. Deposition time was varied to obtain a continuous layer of Cs_2SnI_6 HTM over TNT photo-anode and cell characteristics were studied. We were able to fabricate air stable, all solid-state solar cells with a Jsc of 6 mA/cm^2, Voc of 536 mV and PCE of 1.3%. The study propounds contemporary analysis on Sn based perovskite systems, in the field of DSSCs.

1. Introduction

Recently, there has been a surge of research interest towards developing hybrid organic-inorganic metal halide perovskites for applications in photovoltaics (PV) and other opto-electronic devices [1,2]. This class of hybrid perovskites with general formula AMX_3 consists of a network of corner-sharing MX_6 octahedra, where M atom is a metal cation (eg: Sn^{2+}, Pb^{2+}) and X a halide anion (F^-, Cl^-, Br^-). The A cation balances the net charge of the system and can either be an inorganic species like Cs^+, Rb^+ etc or be small organic molecules like $CH_3NH_3{}^+$ (MA), $CH_3(NH_2)_2{}^+$ (FA) [1,3,4]. Amongst these classes of perovskites, methylammonium lead iodide (MAPI) has generated significant interest with reported photo-conversion efficiencies up to 22.1% [5]. However, with 30% lead content in MAPI there is growing apprehension regarding toxicity of lead-based systems. MAPI based devices also exhibits poor air and moisture stability [6]. There have been several attempts to address these issues by varying the perovskites compositions in order to replace toxic lead with safer materials and also to enhance their stability towards air and moisture, amongst these classes of perovskites [4,6–9].

Lead free all-inorganic perovskites like cesium tin halides ($CsSnX_3$ = Cl, Br, and I) have been reported as materials of interest with applications in various opto-electronic devises [10–12]. $CsSnI_3$ is reported as an efficient hole-transporting material (HTMs), in dye-sensitized solar cells (DSSCs) [10,13,14]. However, $CsSnI_3$ undergoes rapid degradation on exposure to air or moisture due to highly unstable +2 oxidation state of Sn atom [14,15].

Recently, Cs_2SnI_6 a 0-diamentional perovskite derivative with 50% Sn deficiency and with isolated $[SnI_6]^{2-}$ octahedral have been employed as an air stable solid state HTM in DSSCs [15,16]. In a recent study by Kapil et al., Cs_2SnI_6 was reported to be bipolar in nature, *viz;* quite similar to MAPI, Cs_2SnI_6 also exhibits intrinsic electron and hole transport properties and is reported to show p-type conductivity when doped with SnI_2 [17]. Cs_2SnI_6 with Sn atom in Sn^{4+} oxidation state is a semiconductor at room temperature with a band gap of ~1.54 eV [10]. However, the actual valence state of Sn in Cs_2SnI_6 is not yet clearly understood [18]. Notwithstanding this, Cs_2SnI_6 exhibits enhanced stability under ambient air and is reported to be a promising lead free, air and moisture-stable hole transport material [15].

Lee et al. reported ss-DSSC using Cs_2SnI_6 HTM with photo-conversion efficiencies (PCE) of 4.7% using Z907 dye and 7.8% using a mixture of porphyrin dyes [15,16]. Kaltzoglou et al. reported a mixed halide air stable variant; $Cs_2SnI_3Br_3$ HTM based ss-DSSC with PCE of 3.6% using Z907 with additives [19]. In another report, Kaltzoglou et al. studied the stability and ageing of Cs_2SnI_6 HTM based DSSCs under various temperatures and illumination and reported that at room

* Corresponding authors.
E-mail addresses: Lekha@iitb.ac.in (L. Peedikakkandy), pbhargava@iitb.ac.in (P. Bhargava).

https://doi.org/10.1016/j.materresbull.2018.08.046
Received 10 April 2018; Received in revised form 30 August 2018; Accepted 30 August 2018
Available online 31 August 2018
0025-5408/

temperature Cs_2SnI_6 HTM based DSSCs were stable up to several months [20]. Consequently, Cs_2SnI_6 appears particularly promising for large scale module fabrication of stable ss-DSSCs.

All these reports were based on DSSCs with mesoporous titania nanoparticle based photoanodes [15,16,19,20]. Vertically aligned titania nanotubes based DSSCs are reported to show enhanced electron transport properties in comparison to TiO_2 nanoparticulate films [21]. Zhu et al., reported that the charge collection efficiency in TNT-based DSSCs are ~25% higher than the charge collection efficiency of a TiO_2 nanoparticle based DSSC with comparable TiO_2 thickness [22]. But, the use of liquid electrolyte in TNT-DSSC has remained a drawback for its long-term practical application and smooth absorbtion of DSSC into the market. The poor permeability of organic and inorganic hole transport materials into the titania nanotube structures, persists as the major reason for poor cell performances in TNT based SS-DSSCs [23]. This prompted us to investigate application of Cs_2SnI_6 as a solid state HTM in a TNT based DSSCs. In this article, for the first time, we report study of lead free perovskite derivative, Cs_2SnI_6, as a solid state HTM in TNT photoanode based DSSCs. This study opens up new investigations and possibilities to enhance the permeability and improved deposition techniques of Sn based air stable perovskite Cs_2SnI_6 as HTM in TNT based DSSCs. The distinct nature of this study consequently seeks to develop a deeper comprehension and scrutiny, of Sn based perovskite systems.

2. Experimental

2.1. Synthesis of Cs_2SnI_6 crystals

Cs_2SnI_6 was synthesized through precipitation reaction under ambient air conditions. Towards this, 20 mmol aqueous solution of CsI (99.99%,Sigma Aldrich) was prepared and continuously stirred at 70 °C. 30 mmol warm ethanolic solution of SnI_4 (99.99%, Sigma Aldrich) was added into the CsI precursor solution under vigorous stirring leading to precipitation of black crystals of Cs_2SnI_6. Stirring was continued for 30 min till completion of reaction and the product, a black precipitate, was washed with ethanol and separated though centrifugation. Obtained crystals were dried in a hot air oven and stored under ambient conditions.

2.2. Anodization of TNT photoanode

Titania nanotubes were prepared by anodization of Ti foil (0.6 mm thick, 99.2%, TIMET) in ethylene glycol (Merck, 99%) solution containing 0.5 wt% of NH_4F (Merck, 98%) and 2 Vol% DI water at 55 V.

2.3. Fabrication of Cs_2SnI_6 HTM based ss-DSSC

Anodized TNT films were washed in ethanol and annealed at 500 °C for 30 min. Annealed TNT films were dipped into 0.3 mM ethanolic solution of N3 dye (Solaronix) for 12 h. For deposition of Cs_2SnI_6 layer on dye sensitize TNTs, Cs_2SnI_6 HTM solution was prepared. Towards this crystals of Cs_2SnI_6 (50 mg) were dispersed in 1 ml of dimethylformamide (DMF). Further additives like (5 wt%) SnI_2, (1 M) tert-butylpyridine (TBP) and (0.2 M) Li perchlorate were added to the HTM solution to enhance the cell performance [24]. Dye sensitized TNT photoanodes were dipped in Cs_2SnI_6 HTM solution for varying time durations.

Fluorine doped tin oxide (FTO) transparent conductive glass electrodes (10 Ω/cm^2) were cleaned in an ultrasonication bath using soap solution, deionized water, acetone and iso-propanol. The electrodes were coated with Pt nanoparticles solution to prepare transparent conducting counter electrode as reported earlier [25]. Prior assembling the photoanode with counter electrode, a drop of Cs_2SnI_6 HTM solution was casted on to the Pt nanoparticles coated counter electrode for continuity of HTM layer and was pressed onto the photoanode using a 25 μm Surlyn film as a spacer between two electrodes leading to a 0.25 cm^2 photoactive surface. Cells were dried on a hot plate at 80 °C for few minutes and the J–V characteristics studied. Cells were back illuminated as the TNTs were grown on opaque Ti foil.

The samples were analyzed using scanning electron microscope (SEM, JEOL JSM-7600 F FEG-SEM). Energy dispersive X-ray spectroscopy (EDX) coupled with the SEM was used to examine the chemical compositions. X-ray diffraction analysis was carried out with a PANalytical X'Pert Pro with an X'celerator detector. Thermogravimetric studies were carried out by Thermal analysis system (Perkin Elmer, USA). The current-voltage characteristics of solar cells were measured using a Keithley (model 2400) source meter under 100 $mWcm^{-2}$ illumination using a 1000 W Xenon lamp (Newport) as the light source. X-ray Photoelectron Spectroscopy (XPS) measurements of C_2SnI_6 films were performed using a Kratos Axis Supra unit, equipped with monochromated Al Kα X-ray source with a photon energy of 1486.6 eV. Emitted photoelectrons were collected using a concentric hemispherical energy analyzer (Kratos). All measurements were carried out under ultra-high vacuum conditions. XPS data was analyzed using ESCApe software with a Shirley background fitted to the photoelectron peaks acquired.

3. Results and discussions

Crystal structure of synthesized Cs_2SnI_6 powder was investigated using X-Ray diffraction and is displayed in Fig. 1(a). XRD pattern of Cs_2SnI_6 matches with the double perovskite structure (JCPDS No. 51-0466, cubic (space group Fm3m), lattice parameter of 11.627 Å) and matches with the XRD pattern of Cs_2SnI_6 obtained by oxidation of $CsSnI_3$ in air and other synthesis methods. Inset in Fig. 1(a), black aqueous dispersion of Cs_2SnI_6 crystals and a thin film of Cs_2SnI_6 on glass substrate are shown. Fig. 1(b) shows the SEM image of Cs_2SnI_6 crystals.

When recrystallized from organic solvent, Cs_2SnI_6 was found to form large micron size crystals. From Fig. 1(c), thermo-gravimetric analysis of Cs_2SnI_6 powder shows that crystals were stable up to ~80 °C and loses ~20% weight near 150 °C indicating loss of SnI_4 vapors and ~60% weight loss in the vicinity of 270 °C indicating thermal decomposition of Cs_2SnI_6 into CsI. XRD analysis of samples after TGA analysis indicated complete degradation of Cs_2SnI_6 into CsI powder (JCPDS No. 06-0311).

XRD analysis of Cs_2SnI_6 samples stored under ambient conditions does not display impurity peaks upto 10 days and is represented in Fig. 2. Our earlier studies on $CsSnI_3$ indicated that, $CsSnI_3$ undergoes rapid degradation on exposure to moisture and oxygen [14]. The improved air stability of Cs_2SnI_6 is attributed to the stable tetravalent oxidation state of Sn. However, CsI peaks were observed in samples left in air for longer duration (up to 30 days) indicating slow decomposition of Cs_2SnI_6 in air. XPS analysis of fresh and aged Cs_2SnI_6 films exhibits similar results and are included in the supporting information.

Towards solar cell photoanode fabrication, titania nanotubes (TNT) were prepared by anodization of Ti foil. Anodized TNT films were washed in DI water and ethanol and annealed at 500 °C for 30 min. Fig. 3(a) and (b) shows the FE-SEM images of highly-ordered TNT arrays fabricated by anodization of titanium foil. TNT film thickness was estimated by pealing TNTs from the Ti foil using ultra sonication and the thickness of TNT film was estimated to be ~15 μm from FE-SEM images. Fig. 3(c) shows the XRD patterns of TNT after annealing at 500 °C, apart from the peaks of Ti foil (JCPDS No. 44-1294) XRD pattern shows TiO_2 nanotubes to be in anatase phase (JCPDS No. 21-1272).

Dye sensitized TNT photoanodes was dipped in Cs_2SnI_6 HTM solution for varying time durations to deposit Cs_2SnI_6 film over the dye sensitized photo-anode. Fig. 4 shows the SEM images of Cs_2SnI_6 deposition on the dye sensitized TNT photoanode for varying time durations. FE-SEM analysis reveals that Cs_2SnI_6 coverage of TNT photoanode increases with time. After being dipped for 24 h, a continuous

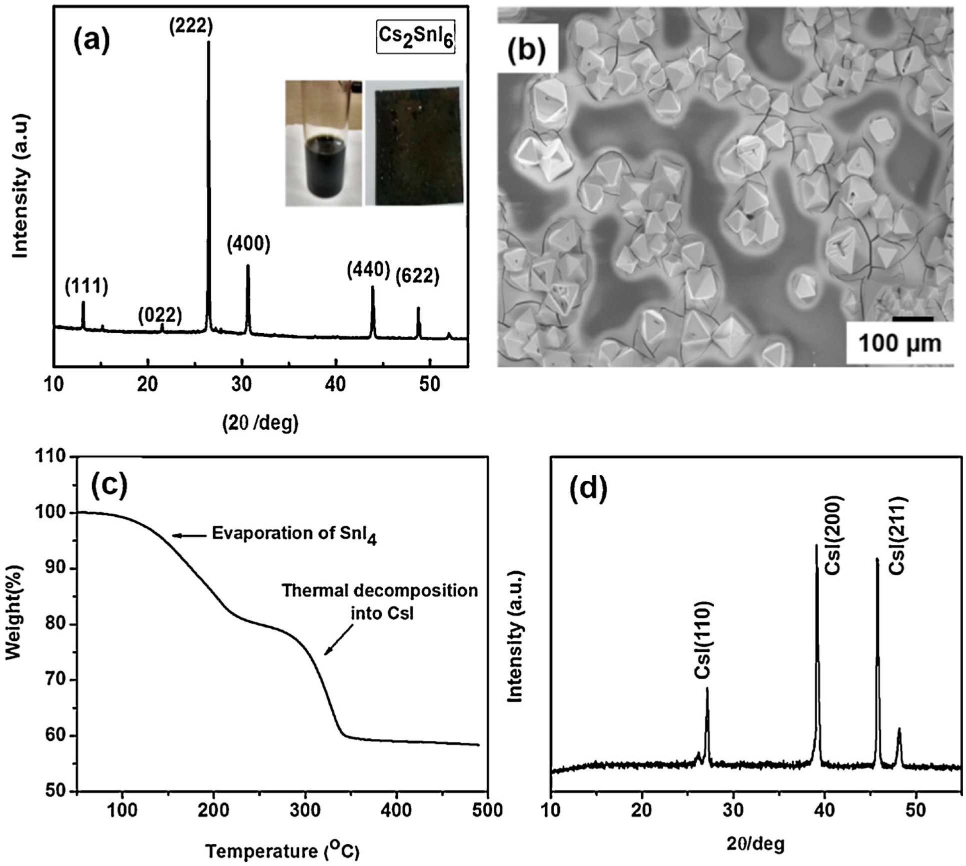

Fig. 1. (a) XRD pattern of Cs_2SnI_6 (JCPDS No. 51-0466) crystals synthesized through precipitation reaction, inset images show solution dispersion and thin film of synthesized Cs_2SnI_6 crystals (b) SEM micrograph of Cs_2SnI_6 synthesized through precipitation reaction (c) Thermogravimetric analysis of Cs_2SnI_6 crystals (d) XRD pattern of Cs_2SnI_6 after thermal degradation.

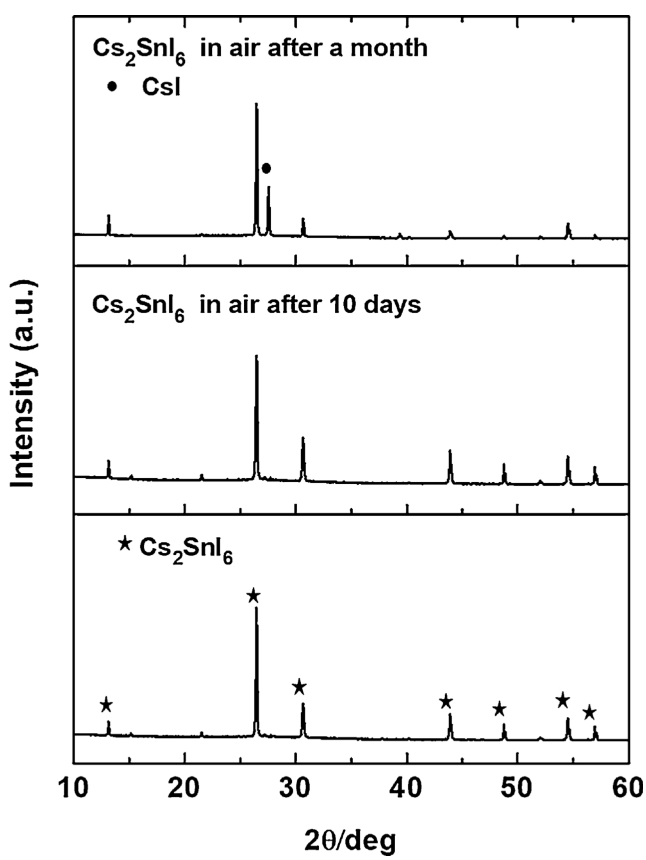

Fig. 2. Powder XRD pattern evolution of Cs_2SnI_6 crystals in air, varying from 0 to 30 days.

film of Cs_2SnI_6 HTM formed over the TNT photoanode. Fig. 5 displays the XRD pattern and EDS analysis of TNT photo-anode sensitized with Cs_2SnI_6 for 24 h.XRD and EDS analysis confirms deposition of Cs_2SnI_6 on TNT photoanode.

Fig. 6(a) and (b) shows the schematic diagram and band gap alignment of back illuminated ss-DSSC device fabricated using dye sensitized TNT photoanode, Cs_2SnI_6 HTM layer and Pt nanoparticle coated counter-electrode. Fig. 6(C) shows the J–V curve of all-solid state DSSCs using Cs_2SnI_6 based HTM with varying deposition time under a simulated illumination of AM 1.5. It was observed that with increased deposition time the photo-conversion efficiency is correspondingly enhanced. Study of J–V characteristics of ss-DSSC with different Cs_2SnI_6 HTM soaking durations indicate that as the loading of HTM into the TNTs increases the Voc and Jsc improves correspondingly. From 2 h up to 24 h soaking time, the Jsc and Voc progressively increases from Jsc-1.5 mA/cm^2&Voc-350 mV to Jsc-6 mA/cm^2 & Voc-540 mV. The solar performance parameters for these devices are displayed in Table 1.

With increasing deposition time, the permeation of Cs_2SnI_6 crystals into the TNT photoanode improves, leading to an intimate contact of HTM with dye molecules and enhanced hole collection efficiency and consequent increase in the cell efficiencies. It was observed that with further increase in HTM deposition time, photocurrent and voltage decreases, possibly be due to reduction in photons reaching the dye molecules due to thicker HTM layers in back illuminated TNT based DSSC. Attaining an optimum thickness of Cs_2SnI_6 HTM layer is therefore crucial in ensuring maximum cell illumination and J–V characteristics. For comparative purposes, we also studied the J–V characteristics of ss-DSSCs with front illuminated, TiO_2 nanoparticles based mesoporous photoanodes of similar TiO_2 layer thickness (Fig. 7(a)). These cells display ~2.1% photo-conversion efficiency with 6 mA/cm^2, Jsc and 525 mV, Voc. J–V characteristics of TNT based DSSCs with liquid electrolyte (iodine/tri-iodide redox couple) was also analyzed

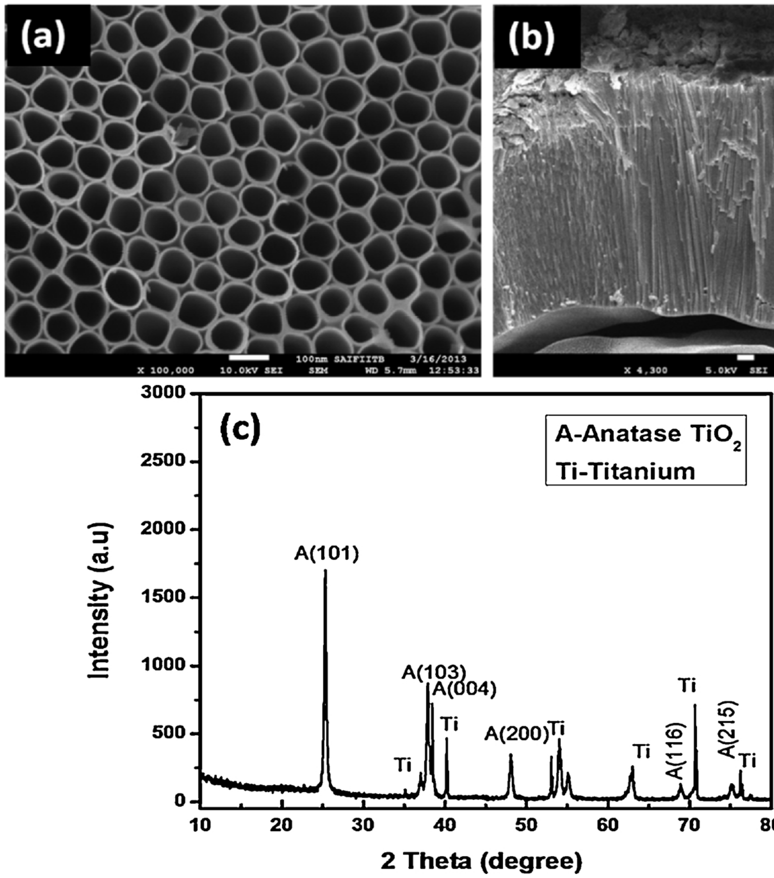

Fig. 3. (a) Top view FE-SEM images of titania nanotubes fabricated through anodization of Ti foil (b) Cross-sectional side view of FE-SEM image of titania nanotubes (c) XRD of titania nano tubes after annealing at 500 °C for 30 min.

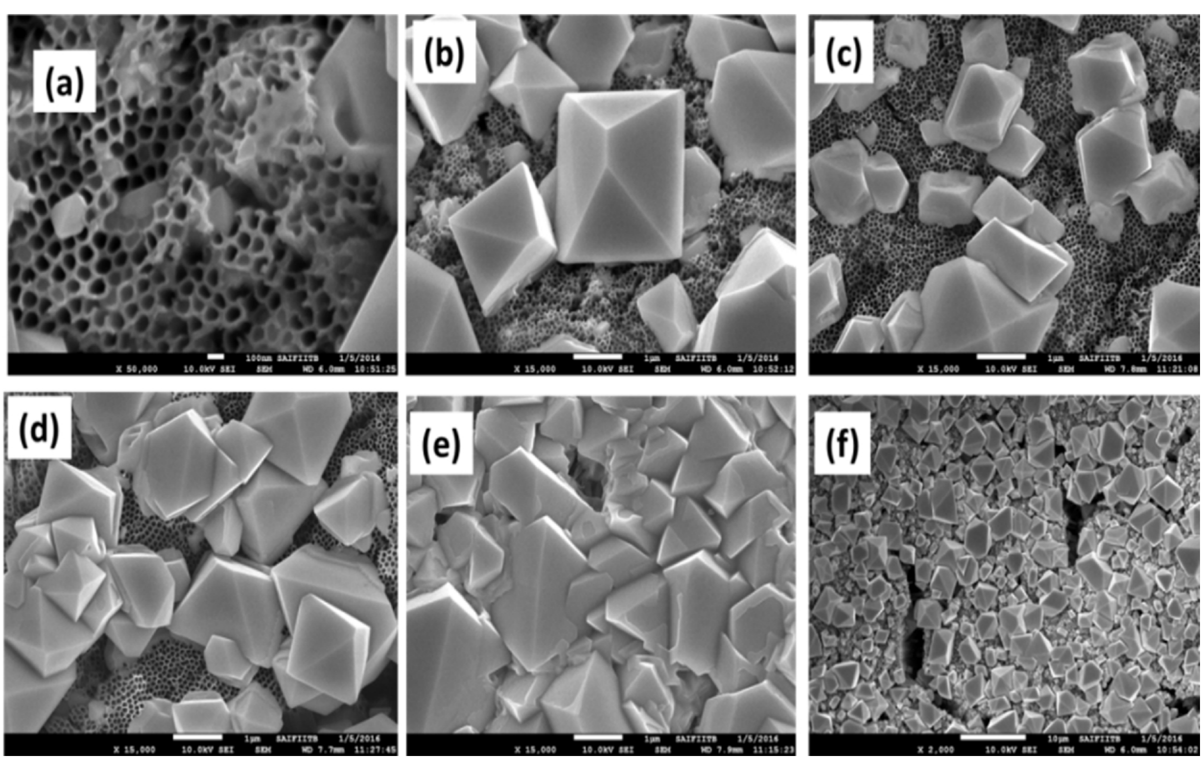

Fig. 4. FE-SEM micrographs of Cs_2SnI_6 HTM layer deposition on TNT nanotubes for different durations (a) 1 h (b) 2 h (c) 6 h (d) 12 h (e) & (f) 24 h.

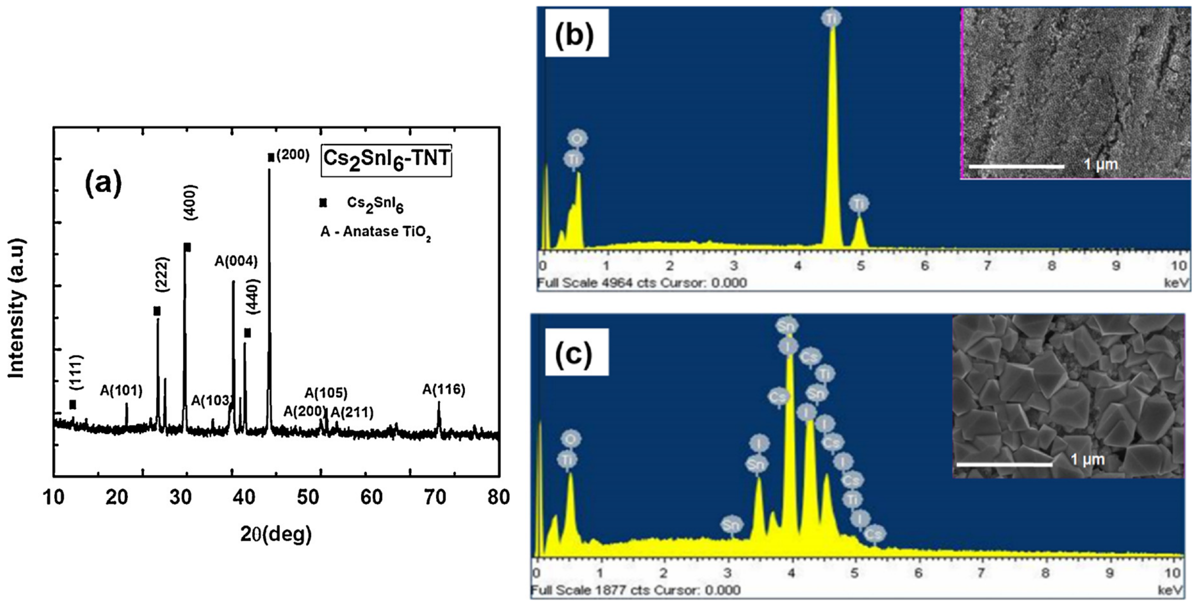

Fig. 5. (a) XRD pattern of Cs_2SnI_6 HTM deposited TNT photoanodes (b) SEM image and EDS analysis of bare TiO_2 nanotube photoanode and (c) SEM image and EDS analysis of TiO_2 nanotube photoanode with Cs_2SnI_6 deposits for 24 h.

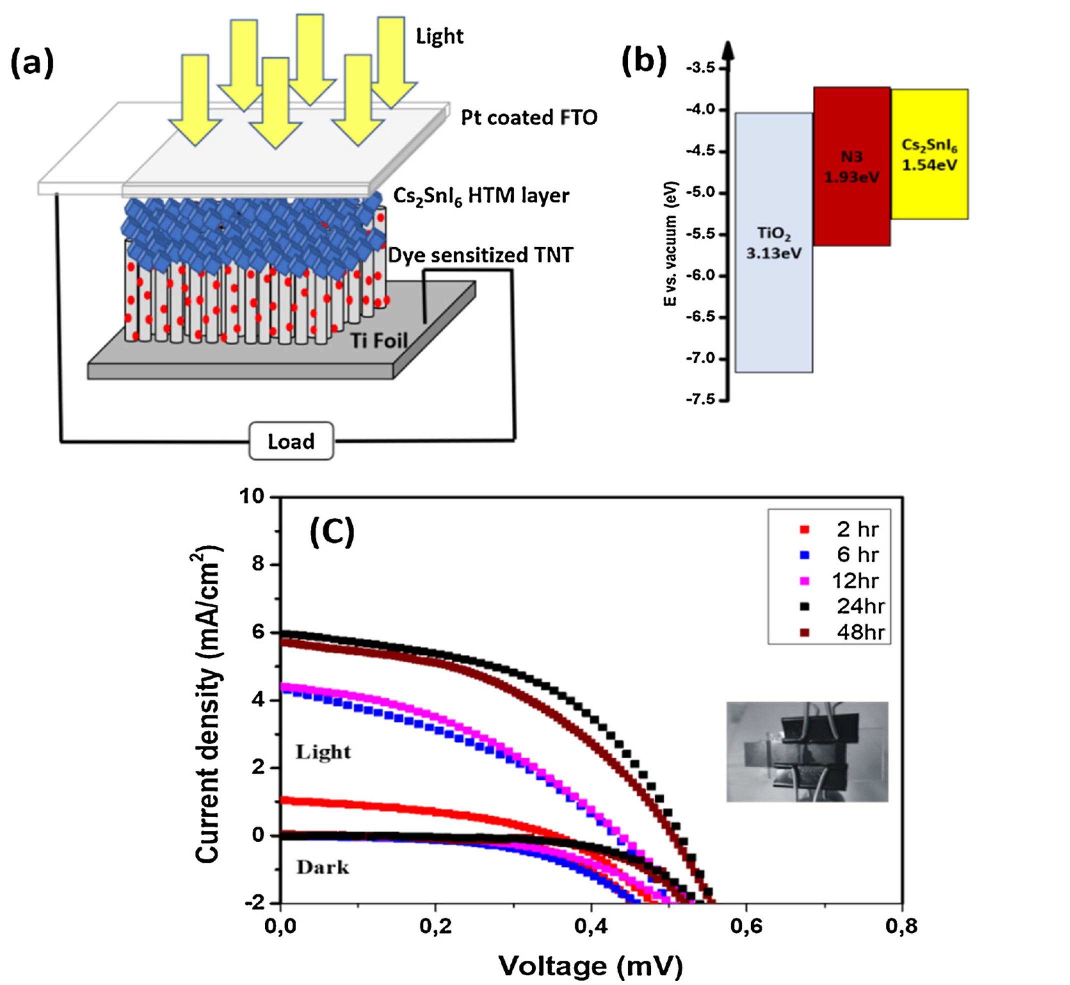

Fig. 6. (a)&(b) Schematic representation and band alignments of the ss-DSSC device (c) Measured J-V characteristics of Cs_2SnI_6 HTM based ss-DSSC with TNT photo-anode soaked in Cs_2SnI_6 HTM for increasing time durations.

Table 1
Performance parameters of DSSC with varying HTMs.

Cs_2SnI_6 HTM deposition time	Jsc (mA/cm^2)	Voc (mV)	FF	η (%)
2 hr	1	345	33	0.1
6 hr	4.3	420	41	0.74
12 hr	4.2	520	39	0.85
24 hr	6	536	40	1.3
48 hr	5.7	520	35	1.03
ss-DSSC with TiO_2 NP photoanode	6	525	67	2.1
TNT-DSSC with I^-/I_3^- liquid electrolyte	9.1	680	54	3.3

(Fig. 7(b)).

Liquid electrolyte based DSSCs exhibits 4% photo-conversion efficiency for similar thickness of TNT photoanode (~15 μm) with a Jsc of 9 mA/cm^2 and Voc 680 mV. Lower Voc and Jsc values of Cs_2SnI_6 HTM based cells compared to liquid electrolyte based system may be primarily attributable to poor permeation of Cs_2SnI_6 layer into the TNT photoanode compared to liquid electrolyte.

The limiting factor for low efficiencies in both TNT based and mesoporous photoanode based DSSCs can be poor permeation of Cs_2SnI_6 crystals into the porous TiO_2 network in the photoanode. Improving the permeation of Cs_2SnI_6 into the dye sensitized photoanode through solvent engineering or two stage vapor deposition methods and also employing TNTs of lower thickness, may lead to higher efficiency cells.

Incident photon to electron conversion efficiency (IPCE) studies shown in Fig. 7(c) indicates that for back illuminated cells the IPCE values are lower for ss-DSSCs than the Iodine/Iodide liquid electrolyte-based cells. This indicates that the thicker layers of HTM reduces the incident light reaching dye molecules resulting in lower efficiencies. Stability of ss-DSSCs with Cs_2SnI_6 HTM under ambient conditions were measured up to 30 days and cells show reduction in performance after ~10 days and is possibly due to decomposition of Cs_2SnI_6 HTM into CsI and SnI_4.

4. Conclusions

Perovskite derivative Cs_2SnI_6 was synthesized using facile solution route method. Crystal structure and stability of samples were studied under ambient conditions using XRD, XPS and thermo-gravimetric analysis. Black crystals of Cs_2SnI_6 were found to be cubic in structure at room temperature and exhibits enhanced stability under ambient air compared to $CsSnI_3$ and thermal stability up to ~80 °C. ss-DSSCs using Cs_2SnI_6 HTM was successfully fabricated using TiO_2 nanotubes as photo-anodes. Using SnI_2 doped Cs_2SnI_6 HTM an efficiency of 1.33% with 40% FF was achieved for 24 h deposition time. Improvement in penetration of Cs_2SnI_6 HTM through solvent engineering or vapor deposition methods can improve the PCE of the cells to realize a low cost, lead free and air-stable solid state solar cell.

Conflicts of interest

There are no conflicts to declare.

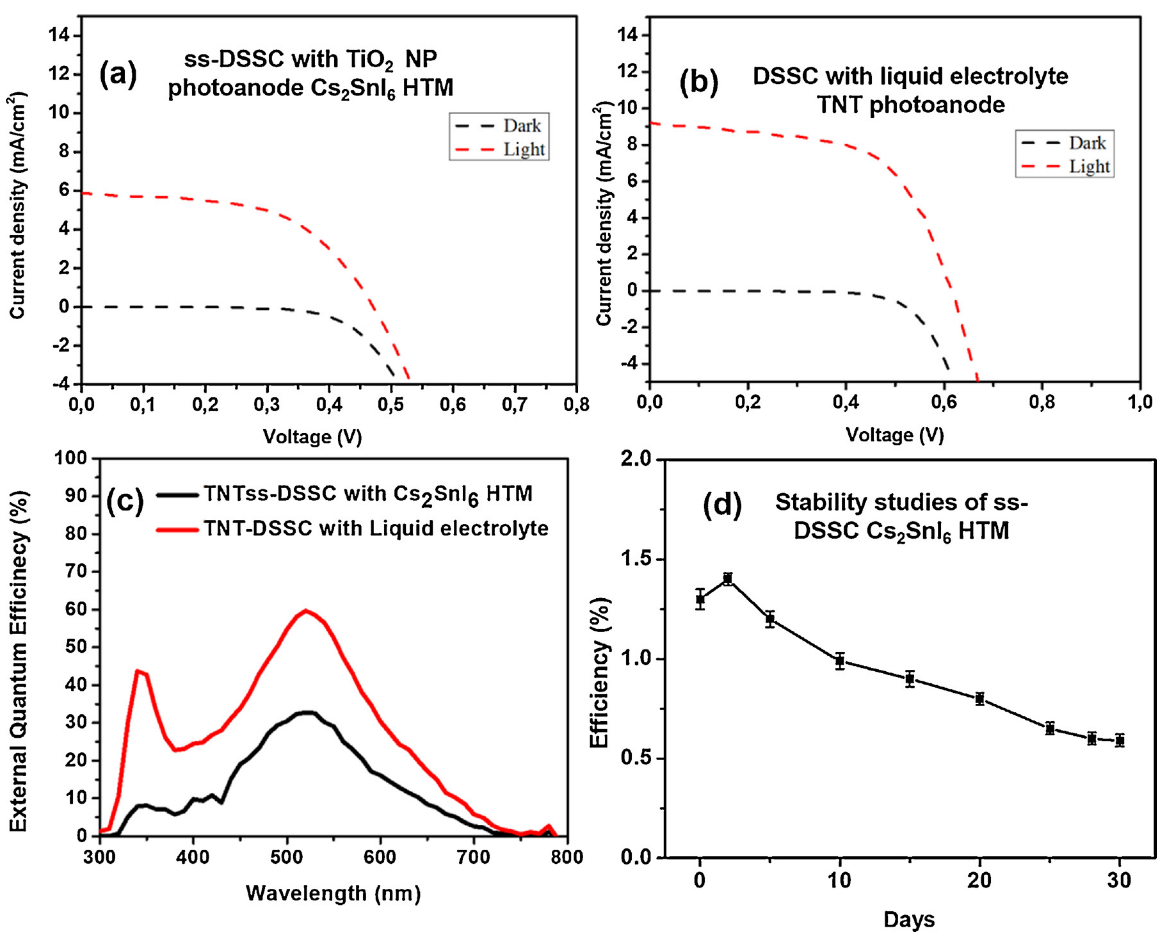

Fig. 7. (a) J-V characteristics of ss-DSSC with TiO_2 nanoparticle based photoanode and Cs_2SnI_6 HTM (b) J-V characteristics of liquid electrolyte based DSSC with TiO_2 nanotube based photoanode (c) External quantum efficiency of TNT based DSSCs with liquid electrolyte and Cs_2SnI_6 HTM and (d) Stability studies of ss-DSSCs with Cs_2SnI_6 HTM.

Acknowledgments

The authors acknowledge financial support from the Department of Science and Technology of India (SR/S3/ME/0017/2009) and the Solar Energy Research Institute for India and the United States (SERIIUS) and SAIF (IIT-B) for SEM images of crystals.

References

[1] M.A. Green, A. Ho-Baillie, H.J. Snaith, The emergence of perovskite solar cells, Nat. Photonics 8 (2014) 506–514, https://doi.org/10.1038/nphoton.2014.134.

[2] H.-S. Kim, C.-R. Lee, J.-H. Im, K.-B. Lee, T. Moehl, A. Marchioro, S.-J. Moon, R. Humphry-Baker, J.-H. Yum, J.E. Moser, M. Grätzel, N.-G. Park, Lead iodide perovskite sensitized all-solid-state submicron thin film mesoscopic solar cell with efficiency exceeding 9%, Sci. Rep. 2 (2012) 591, https://doi.org/10.1038/srep00591.

[3] B. Saparov, D.B. Mitzi, Organic–inorganic perovskites: structural versatility for functional materials design, Chem. Rev. 116 (2016) 4558–4596, https://doi.org/10.1021/acs.chemrev.5b00715.

[4] S. Yang, W. Fu, Z. Zhang, H. Chen, C.-Z. Li, Recent advances in perovskite solar cells: efficiency, stability and lead-free perovskite, J. Mater. Chem. A 5 (2017) 11462–11482, https://doi.org/10.1039/C7TA00366H.

[5] W.S. Yang, B.-W. Park, E.H. Jung, N.J. Jeon, Y.C. Kim, D.U. Lee, S.S. Shin, J. Seo, E.K. Kim, J.H. Noh, S. Il Seok, Iodide management in formamidinium-lead-halide–based perovskite layers for efficient solar cells, Science 356 (2017) 1376–1379, https://doi.org/10.1126/science.aan2301.

[6] S. Chatterjee, A.J. Pal, Influence of metal substitution on hybrid halide perovskites: towards lead-free perovskite solar cells, J. Mater. Chem. A 6 (2018), https://doi.org/10.1039/C7TA09943F.

[7] F. Hao, C.C. Stoumpos, D.H. Cao, R.P.H. Chang, M.G. Kanatzidis, Lead-free solid-state organic-inorganic halide perovskite solar cells, Nat Phot. 8 (2014) 489–494, https://doi.org/10.1038/nphoton.2014.82.

[8] S. Chakraborty, W. Xie, N. Mathews, M. Sherburne, R. Ahuja, M. Asta, S.G. Mhaisalkar, Rational design: a high-throughput computational screening and experimental validation methodology for lead-free and emergent hybrid perovskites, ACS Energy Lett. 2 (2017) 837–845, https://doi.org/10.1021/acsenergylett.7b00035.

[9] P.K.Singh Rahul, R. Singh, V. Singh, B. Bhattacharya, Z.H. Khan, New class of lead free perovskite material for low-cost solar cell application, Mater. Res. Bull. 97 (2018) 572–577, https://doi.org/10.1016/j.materresbull.2017.09.054.

[10] I. Chung, J.-H. Song, J. Im, J. Androulakis, C.D. Malliakas, H. Li, A.J. Freeman, J.T. Kenney, M.G. Kanatzidis, CsSnI3: semiconductor or metal? High electrical conductivity and strong near-infrared photoluminescence from a single material. High hole mobility and phase-transitions, J. Am. Chem. Soc. 134 (2012) 8579–8587, https://doi.org/10.1021/ja301539s.

[11] T.C. Jellicoe, J.M. Richter, H.F.J. Glass, M. Tabachnyk, R. Brady, S.E. Dutton, A. Rao, R.H. Friend, D. Credgington, N.C. Greenham, M.L. Böhm, Synthesis and optical properties of lead-free cesium tin halide perovskite nanocrystals, J. Am. Chem. Soc. 138 (2016) 2941–2944, https://doi.org/10.1021/jacs.5b13470.

[12] L. Dimesso, C. Das, M. Stöhr, W. Jaegermann, Investigation of cesium tin/lead iodide (CsSn1 − xPbxI3) systems, Mater. Res. Bull. 85 (2017) 80–89, https://doi.org/10.1016/j.materresbull.2016.08.052.

[13] N. Chander, P.S. Chandrasekhar, V.K. Komarala, Solid state plasmonic dye sensitized solar cells based on solution processed perovskite CsSnI3 as the hole transporter, RSC Adv. 4 (2014) 55658–55665, https://doi.org/10.1039/C4RA09719J.

[14] L. Peedikakkandy, P. Bhargava, Recrystallization and phase stability study of cesium tin iodide for application as a hole transporter in dye sensitized solar cells, Mater. Sci. Semicond. Process. 33 (2015) 103–109, https://doi.org/10.1016/j.mssp.2015.01.023.

[15] X. Qiu, B. Cao, S. Yuan, X. Chen, Z. Qiu, Y. Jiang, Q. Ye, H. Wang, H. Zeng, J. Liu, M.G. Kanatzidis, From unstable CsSnI3 to air-stable Cs_2SnI_6: a lead-free perovskite solar cell light absorber with bandgap of 1.48 eV and high absorption coefficient, Sol. Energy Mater. Sol. Cells 159 (2017) 227–234, https://doi.org/10.1016/j.solmat.2016.09.022.

[16] B. Lee, C.C. Stoumpos, N. Zhou, F. Hao, C. Malliakas, C. Yeh, T.J. Marks, M.G. Kanatzidis, R.P.H. Chang, Air-stable molecular semiconducting iodosalts for solar cell applications: Cs_2SnI_6 as a hole conductor, J. Am. Chem. Soc. 136 (2014) 15379–15385, https://doi.org/10.1021/ja508464w.

[17] G. Kapil, T. Ohta, T. Koyanagi, M. Vigneshwaran, Y. Zhang, Y. Ogomi, S.S. Pandey, K. Yoshino, Q. Shen, T. Toyoda, M.M. Rahman, T. Minemoto, T.N. Murakami, H. Segawa, S. Hayase, Investigation of interfacial charge transfer in solution processed Cs_2SnI_6 thin films, J. Phys. Chem. C 121 (2017) 13092–13100, https://doi.org/10.1021/acs.jpcc.7b04019.

[18] Z. Xiao, Y. Zhou, H. Hosono, T. Kamiya, Intrinsic defects in a photovoltaic perovskite variant Cs_2SnI_6, Phys. Chem. Chem. Phys. 17 (2015) 18900–18903, https://doi.org/10.1039/C5CP03102H.

[19] A. Kaltzoglou, M. Antoniadou, D. Perganti, E. Siranidi, V. Raptis, K. Trohidou, V. Psycharis, A.G. Kontos, P. Falaras, Mixed-halide $Cs_2SnI_3Br_3$ perovskite as low resistance hole-transporting material in dye-sensitized solar cells, Electrochim. Acta 184 (2015) 466–474, https://doi.org/10.1016/j.electacta.2015.10.030.

[20] A. Kaltzoglou, D. Perganti, M. Antoniadou, A.G. Kontos, P. Falaras, Stress tests on dye-sensitized solar cells with the Cs_2SnI_6 defect perovskite as hole-transporting material, Energy Procedia 102 (2016) 49–55, https://doi.org/10.1016/j.egypro.2016.11.317.

[21] H.-P. Jen, M.-H. Lin, L.-L. Li, H.-P. Wu, W.-K. Huang, P.-J. Cheng, E.W.-G. Diau, High-performance large-scale flexible dye-sensitized solar cells based on anodic TiO2 nanotube arrays, ACS Appl. Mater. Interfaces 5 (2013) 10098–10104, https://doi.org/10.1021/am402687j.

[22] K. Zhu, N.R. Neale, A. Miedaner, A.J. Frank, Enhanced charge-collection efficiencies and light scattering in dye-sensitized solar cells using oriented TiO2 nanotubes arrays, Nano Lett. 7 (2007) 69–74, https://doi.org/10.1021/nl062000o.

[23] C.-H. Tsai, Y.-L. Chen, H.-L. Hsu, Y.-R. Ma, S. Mou, Enhancing the efficiency of quasi-solid-state dye-sensitized solar cells by adding bis(trifluoromethane)sulfonimide lithium salt and camphorsulfonic acid to gel-based electrolytes, Mater. Res. Bull. 107 (2018) 87–93, https://doi.org/10.1016/j.materresbull.2018.07.017.

[24] J. Ye, L. Zhou, L. Zhu, X. Zhang, Z. Shao, X. Pan, S. Dai, Bipyridine type Co-complexes as hole-transporting material dopants in perovskite solar cells, RSC Adv. 6 (2016) 17354–17359, https://doi.org/10.1039/C5RA25753K.

[25] G. Calogero, P. Calandra, A. Irrera, A. Sinopoli, I. Citro, G.Di Marco, A new type of transparent and low cost counter-electrode based on platinum nanoparticles for dye-sensitized solar cells, Energy Environ. Sci. 4 (2011) 1838–1844, https://doi.org/10.1039/C0EE00463D.